Proc. Natl. Acad. Sci. USA
Vol. 82, pp. 3626–3630, June 1985
Biochemistry

Monomers through trimers of large tumor antigen bind in region I and monomers through tetramers bind in region II of simian virus 40 origin of replication DNA as stable structures in solution

(scanning transmission electron microscopy/mass distribution within a bound oligomer/G-A-G-G-C recognition sequence)

IRIS A. MASTRANGELO*, PAUL V. C. HOUGH†, VAN G. WILSON*‡, JOSEPH S. WALL†, JAMES F. HAINFELD†, AND PETER TEGTMEYER*

*Department of Microbiology, State University of New York at Stony Brook, Stony Brook, NY 11794; and †Biology Department, Brookhaven National Laboratory, Upton, NY 11973

Communicated by Cyrus Levinthal, February 15, 1985

ABSTRACT **Large tumor (T) antigen and its bound multimeric states are positioned by scanning transmission electron microscopy (STEM) within a few base pairs at control sequences of the simian virus 40 DNA origin of replication region. Proximal and distal edge positions for each multimer group match the end positions of previously mapped fragments protected from DNase cleavage. Since chance correspondence is shown to be extremely unlikely, STEM mass measurements, obtained concurrently with STEM map positions, indicate that the DNase fragments arise from bound monomers, dimers, trimers, and tetramers in binding region II and monomers, dimers, and trimers in binding region I. Simultaneous binding of seven monomer-equivalent masses is observed, three in region I and four in region II, with an ordered and interpretable mass distribution in the plane of the foil. Although this observation does not prove that the six G-A-G-G-C and one T-A-G-G-C sequences, similarly distributed, function as recognition sequences for T-antigen monomer, it provides strong support for such a model. The stable existence in solution of low- and intermediate-mass structures, observed at lower T-antigen concentrations, suggests a role as assembly intermediates.**

The simian virus 40 (SV40) gene *A* product, large tumor (T) antigen, is required for viral replication (1, 2) and represses early transcription late in productive infection (3, 4; for recent reviews, see refs. 5–7). Experiments to determine the mechanisms of regulation by T antigen have attacked successfully the problem of identifying the DNA sequences with which the protein interacts (8–15) but less definitively the characterization of bound structures (16–19).

Restriction fragment lengths in the range of a few hundred base pairs (bp) are now measured—unstained, unshadowed, and on uncoated thin carbon film—with a SD of 2–3% by scanning transmission electron microscopy (STEM) (ref. 20; unpublished data). The well-established theory of errors for STEM mass measurement (21–23) has been shown to apply in the case of protein bound to DNA (20). Thus STEM can provide position ("footprinting") information at only slightly lower precision than biochemical techniques and concurrently can measure the protein mass bound. Further, the data as recorded determine the mass in 10×10 Å^2 or 5×5 Å^2 areas.

Previous work (8–11) has established that T antigen binds most strongly in region I at the early-transcription side of the origin of replication (see Fig. 1). It binds less strongly in region II, centered on the 27-bp palindrome within the essential origin of replication. Binding in region II is required for initiation of replication (26, 27); maximal repression of early transcription seems to require simultaneous binding in regions I and II (28, 29). T antigen also binds weakly in region III, roughly coincident with the 21-bp repeats (Fig. 1) (30, 31) at the late-transcription side of the origin; its functional role in III is not yet known (32). DNase protection experiments (8–10, 12), DNase and dimethyl sulfate cleavage inhibition patterns ("footprints") (8, 12–14), and alkylation-interference experiments (15) have been used to explore the binding interactions of T antigen with respect to origin sequences in considerable detail. A model has been proposed in which monomer units (12) recognize the pentanucleotide 5′ G(T)-A-G-G-C 3′ in binding regions I and II and 5′ G(T)-G-G-G-C 3′ in binding region III (Fig. 1) (8, 12, 13). However, efforts to determine the multimeric state of the protein before or after binding have led as yet to no real consensus. Approaches have included assay of fractionated oligomers for DNA binding using several biochemical methods (17–19, 33) and conventional electron microscopy of stained and shadowed preparations (16).

We report STEM map positions and mass distributions for some 60 individual binding events occurring *in vitro* on wild-type DNA and on a control mutant lacking binding region I. In combination with earlier biochemical protection experiments, they establish the stable existence in solution of specifically bound monomers, dimers, trimers, and tetramers and suggest that the more complex structures assemble through successive binding to recognition pentanucleotides.

MATERIALS AND METHODS

T-Antigen Purification. Gene *A* protein was purified 1000-fold to 20–40% purity from CV-1 cells as described (34). Control extracts purified by identical means from uninfected cells had no origin-specific binding capability, judged both microscopically and by DNase protection assays.

Specimen Preparation. Binding reactions contained 7–70 ng of T antigen and 30–180 ng of *Ava* II D fragment DNA in a 20-μl reaction volume; binding buffer was 20 mM Pipes, pH 7.0/3 or 75 mM NaCl/0.1 mM EDTA/5 mM $MgCl_2$/10% glycerol. The molar ratio of T-antigen monomer to *Ava* II D fragment was 12, 1, or 0.2. After a 1-hr incubation at 4°C, 3 mM glutaraldehyde was added to crosslink complexes. Complexes were diffused to grids directly from reaction mixes or were first separated from unbound protein on a 1-ml column of Bio-Rad A-5m. Void-volume fractions were centrifuged to grids in modified Miller chambers (20). Subsequent procedures have been described (20).

The publication costs of this article were defrayed in part by page charge payment. This article must therefore be hereby marked "*advertisement*" in accordance with 18 U.S.C. §1734 solely to indicate this fact.

Abbreviations: STEM, scanning transmission electron microscopy; T antigen, tumor antigen; bp, base pair; SV40, simian virus 40.

‡Present address: Department of Medical Microbiology and Immunology, Texas A & M Univ., College Station, TX 77843.

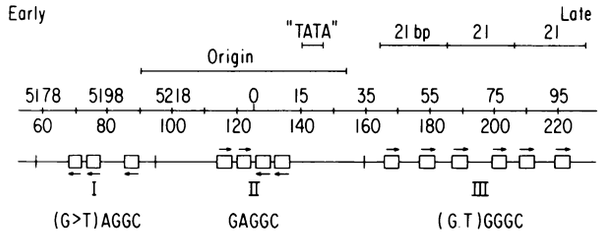

Fig. 1. Some landmarks of the SV40 regulatory region. Sequence numbers above the line are according to the standard system of Buchman *et al.* (24); below the line they are distances in bp from the early-transcription end of *Ava* II D fragment. Limits of T-antigen-binding regions I–III were determined by DNase protection and cleavage inhibition pattern experiments (12, 13). Boxes show locations of approximately homologous pentanucleotides, oriented as arrows indicate. Also indicated are the essential origin of replication (25) and the "TATA" box and 21-bp repeats, control sequences for early transcription (5). Early transcripts are synthesized toward the left in the diagram.

STEM (35). In the present work, the probe matrix was 1 × 1 nm^2 or 0.5 × 0.5 nm^2. Stage temperature was −140°C. Molecules analyzed received electron doses of 10–40 electrons per $Å^2$ (40%), 40–55 (50%), and 55–95 (10%). Over this dose range, mass loss of tobacco mosaic virus, used for calibration, accurately compensates for mass loss in bound protein (35, 36).

Data Analysis. Contour lengths for the 684-bp *Ava* II D fragments were measured by a Numonics graphics calculator. A conversion factor derived from these and other length measurements, 3.00 ± 0.03 bp/nm, was used to determine protein position with respect to the known *Ava* II D sequence. Over the range 300–1000 bp, the observed fractional SD in measured length was 2.0%. For shorter lengths a constant SD of 5 bp, based largely on theoretical considerations of resolution and end denaturation, was applied. DNA contact length was measured as a straight line between proximal and distal protein edges; this assumed no deviation in the DNA path.

Error in total mass (protein mass plus carbon substrate) derives from the counting statistical error for scattered electrons. SD in substrate mass was taken as the SD for 10 neighboring areas. The resultant fractional error for a protein of T-antigen monomer size, 82 kDa, was 8–10%. In addition, the mass calibration constant determined by measurement of tobacco mosaic virus showed an experimental SD of 4–6%, which we combine in quadrature.

Except for end-binding, the STEM observations showed negligible binding of T antigen at nonspecific sites.

RESULTS

Identification of Bound Oligomers. STEM mass measurement is based on a proportionality, established in classical electron-scattering experiments (37), between the mass of a constituent atom in a macromolecule and the number of incident electrons scattered by it. Fig. 2 shows the measured mass distribution for protein structures bound in regions I through III. The distribution is well fit by gaussian distributions at 1, 2, and 3 × 82 kDa. The six measured masses plotted above 290 kDa are all consistent with a gaussian distribution whose mean is 4 times the lowest mean mass (see the legend to Fig. 2). A few higher multiples of monomer mass were observed: a hexamer in region I and an octamer in region II on wild-type DNA and an aggregate, mass about dodecamer, in region II of cs1097. Their relative infrequency indicates that they are not major binding forms, and consequently, they were not considered further.

The SV40 DNA sequence predicts a monomer molecular mass of 81,632 daltons for T antigen (24). We conclude that monomer through tetramer masses are bound in the origin regions.

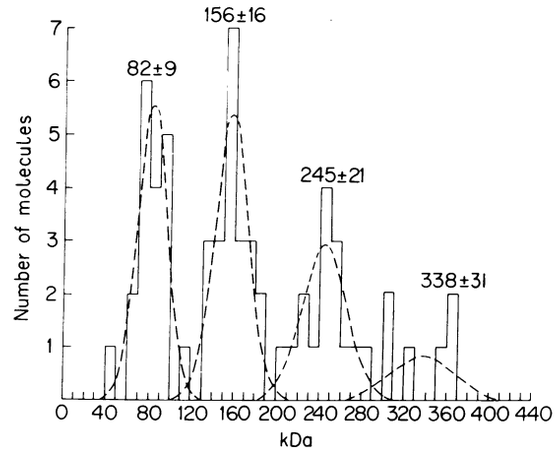

FIG. 2. Molecular mass, measured by STEM for structures bound in regions I–III (Fig. 1). Histogram of measured masses, and gaussian fits, with mean and SD as shown at each peak (UCLA BMDP-AR programs). The six masses above 300 kDa have a mean ± SD of 338 ± 31 kDa and, thus, are compatible with a single tetramer mass of 4 × 82 = 328 kDa. Inclusion of this gaussian fit reduces χ^2 in the overall trimer–tetramer region significantly ($P < 0.1$). Errors from the fit are in good agreement with predicted errors from STEM theory (see *Materials and Methods*).

Mass Distributions, as Projected onto the Plane of the Foil, for Monomers, Dimers, Trimers, and Tetramers. An example of a STEM micrograph generated from untreated scattering data is reproduced in Fig. 3. When the data were locally averaged, interpolated, and represented as a color-coded contour map, the results of Fig. 4 *A–D* were obtained, showing a progression of monomer through tetramer. More variability in images for a given multimer than is suggested by this progression occurred owing to the different possible aspects of each multimer as projected onto the foil. Each oligomer in Fig. 4 can be visualized as constructed of lower-mass oligomers, if a 90° rotation of lower oligomers about the DNA

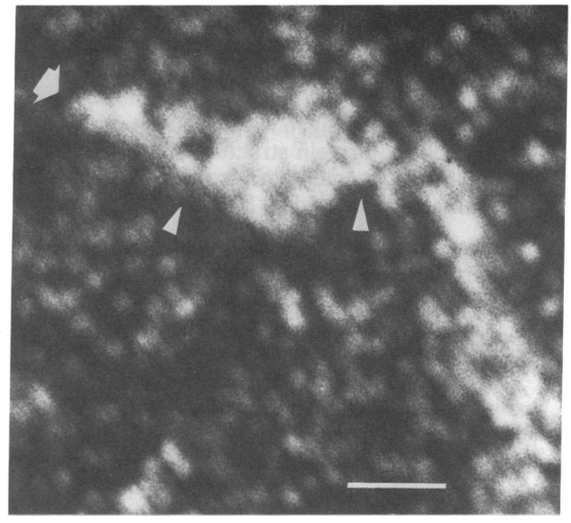

FIG. 3. STEM darkfield image of T-antigen dimer in region I. Probe matrix = 1.0 × 1.0 nm^2. Increased white means higher scattered electron number. The dimer has a proximal edge at 50 bp and a distal edge at 95 bp (triangles), measured from the closer end of a wild-type DNA restriction fragment (arrow). (Bar = 30 bp or 10 nm.)

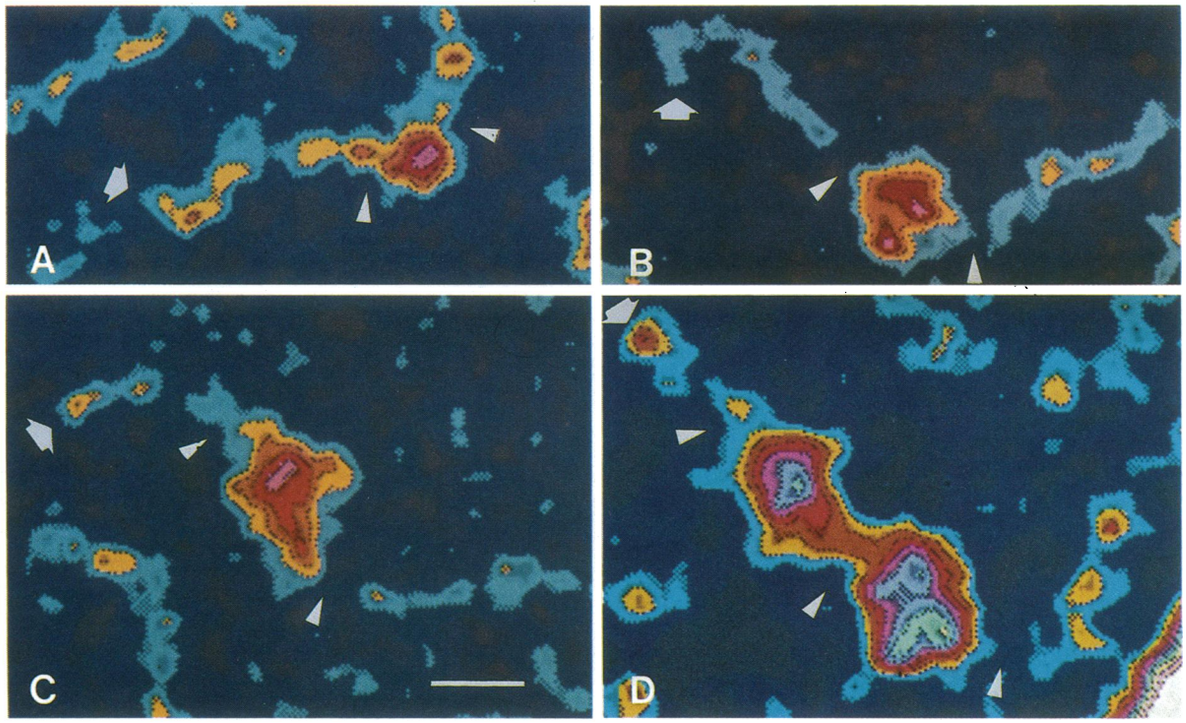

FIG. 4. STEM digital images processed by local averaging (38) and bilinear interpolation (39) and represented by color-coded contour maps. The weighting function used in averaging reduces the counting statistical errors by a factor of 3. Low-attention colors, dark gray and blue, are chosen to represent substrate (carbon foil). For succeeding increments of 5 in electron count, the color progresses through cyan, yellow, orange, red, magenta, pastel blue, pastel green, pastel yellow, and pastel magenta to white. In each frame, the *Ava* II D fragment end is marked with a white arrow, and the edges of the oligomer are marked by white triangles. (Bar = 30 bp or 10 nm.) (*A*) Monomer in region I. (*B*) Dimer in region II. (*C*) Trimer in region II. (*D*) Trimer in region I with tandem tetramer in region II. Fragments in *A* and *D* are wild-type DNA; fragments in *B* and *C* are cs1097 DNA (25).

axis is allowed. An alternative representation of mass distributions, Fig. 5, shows a computer-constructed perspective drawing of the trimer/tetramer of Fig. 4*D* in which height above the plane is proportional to mass thickness. Adding up the block heights gives the mass in any part, and by this means one can divide the structure into two dimers making up the tetramer and a similar dimer with monomer appendage making up the trimer.

STEM Map Positions: Location and Contact Lengths of Bound Oligomers. The significance of a contact length and of edge positions relative to an *Ava* II D fragment end can perhaps best be judged from actual micrographs such as those of Figs. 3–5. Binding regions I and II were normally clearly separate, as in Fig. 5. In Fig. 6 we plotted the positions of the edges of each bound protein structure relative to the closer end of the *Ava* II D fragment and grouped the structures according to mass as measured by STEM. Five binding events

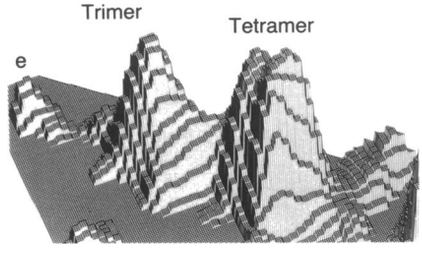

FIG. 5. Three-dimensional perspective drawing of the mass distributions for a T-antigen trimer in binding region I and a tandem tetramer in binding region II. Individual blocks making up the structure represent 1 × 1 nm^2 STEM picture elements and have a height representing the electron count for that element minus a constant foil background.

observed in the low-affinity region III are too few to contribute significantly to the analysis by region in Fig. 6. We observed monomers through trimers in region I, monomers through tetramers in region II, and monomers through trimers in region III.

Edge variations (Fig. 6) for masses located in a single region (solid bars), spanning regions I and II (alternating solid and open bars), and bound to mutant cs1097 deleted for region I (open bars) were compatible with a 5-bp SD in contour length (see *Materials and Methods*). Assignment of each oligomer to region I or II is unambiguous. With few exceptions, the assignment of each binding structure to a multimeric state of T antigen also is unambiguous (Fig. 2). Therefore, each occurrence of a compact grouping of edge position and contact length is independent evidence for specificity of binding.

Our experiment design, in particular crosslinking in solution before deposition on grids, attempts to preserve all binding events. Under our conditions, T antigen favored binding region I over binding region II by about 2:1. The macromolecular concentrations we used are relatively high to increase event density on the grid; a major component of our observed binding in region II occurred, for example, in a reaction with DNA fragment concentration 3 nM and T antigen monomer concentration 40 nM. Some experiments, based on filter binding or antibody precipitation of deletion mutants, have measured a binding-event ratio of 10 or more (14, 26). Results of other methods comparing relative binding to regions I and II on the same DNA fragment agree with our binding ratios. DNase cleavage protection patterns (26), nuclease protection (40), and dimethyl sulfate protection patterns (unpublished data) have shown onset of protection for region II at 2 to 3 times the protein concentration required for onset of region I protection.

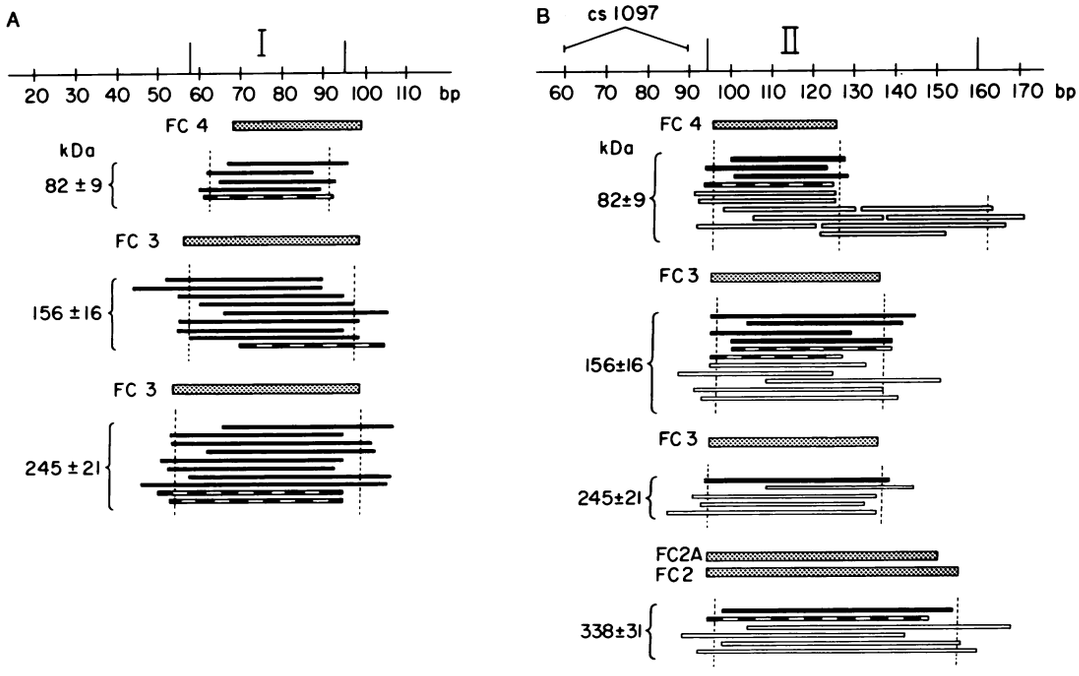

FIG. 6. Binding positions and contact lengths of T-antigen multimers in binding regions I and II. Numbers for wild-type DNA show the distance in bp from the *Ava* II D fragment end. (*B*) Region I, bp 60–90, is deleted in cs1097 DNA (25). Mutant and wild-type DNA are aligned for sequences beginning with bp 91. Structures on wild-type DNA (solid bars) occur on different *Ava* II D fragments. Alternating open and solid bars depict mass distributions spanning regions I and II on wild-type DNA. Open bars show binding to cs1097 DNA. Structures are grouped according to the gaussian fits of Fig. 2; mean mass is indicated. Mapped positions and fragment lengths from earlier DNase protection experiments (12) are reproduced as stippled bars for comparison with STEM positions; they are labeled fragment classes (FC) 2, 2A, 3, and 4 as designated previously (12). Vertical dotted lines mark mean positions of proximal and distal edges in each mass group; SEMs are: ± 1.5 bp for monomers, ± 2 bp for dimers, ± 2–3.5 bp for trimers, and ± 2 and 4 bp for tetramers. In three cases on cs1097 DNA (region II, open bars), a pair of monomers occurs on the same fragment, occupying the entire region. We have indicated the mean distal edge position for the distal monomer of each pair and the single monomer bound in the distal part of the region II. In wild-type DNA, a fragment class has not been identified that maps to the distal half of region II. If DNase does not cut between monomer pairs, the protected fragment would be similar to FC2. For the seven multimer groups (*A* and *B*) proximal edges observed by STEM could have occurred at any distance between 0 and 340 bp measured to the closest end. The probability of any one agreement by chance with a left end of a mapped DNase protection assay fragment is roughly (6/340) ≃ (2/100), where "6" is $2 \times (SD_1^2 + SD_2^2)^{1/2}$, with SD_1 as the STEM protein edge SD and SD_2 as the DNase fragment end SD. Actually, the first STEM monomer edge could agree by chance with the shortest DNase fragment end from either region I or II, increasing the probability by 2; the second monomer edge must agree, however, with exactly the other fragment end. The probability that all seven proximal edges agree is then $(2/100)^7 \simeq 10^{-12} \times 2^4$, or $\approx 10^{-11}$.

Comparison of STEM Contact Lengths and Positions with DNase Protection Assay Fragments. In principle, STEM map positions and DNase protection assay fragments each determine the extent of a bound protein structure and the position of its proximal and distal edges relative to a restriction fragment end.

Previous work (12) has established the fragment classes protected from DNase cleavage, shown as stippled bars in Fig. 6, and has mapped them to the sequence locations shown. Measured lengths for a given class vary over a range of about 5 bp (equivalent to a SD of 2–3 bp), reflecting perhaps both alternative enzyme cutting sites and a dynamic interaction between T antigen and DNA. Vertical dotted lines in Fig. 6 indicate the mean position for the proximal and distal edges of each group of multimers as measured by STEM. The SEM for each mean edge position is 2–4 bp (see the legend to Fig. 6), comparable with DNase fragment errors. Comparison of the STEM and DNase protection measurements shows mainly <1 and very occasionally 2 SD differences and, therefore, excellent agreement in map locations.

Mean edge positions and contact length for trimers in region II were not significantly different from the corresponding positions and length for dimers. Addition of a monomer mass to an existing dimer with little or no increase in contact length implies an addition has occurred between the limits of dimer mass, for example in the major groove on the opposite face of the helix. The trimer of Fig. 4*C* is 10 bp longer than the mean trimer length in region II. It may be interpreted as monomer mass addition outside the dimer. Mass addition must occur in both places finally to account for the observed contact length of region II tetramers. Since DNase protection experiments do not measure mass, it is reasonable that they find only one, presumably heterogeneous, fragment class that coincides with STEM dimers and trimers in region II.

In region I, the STEM mean contact length for trimers is about 5 bp greater than for dimers. However, recognizing the presence of these two groups by DNase protection alone without the mass measurement would again be difficult.

In Fig. 6 *A* and *B*, seven proximal edges observed by STEM agree with left ends of six mapped DNase protection assay fragments within rather small errors. The probability that such agreement occurred by chance is 10^{-11} or less (see the legend of Fig. 6). Thus, we may conclude that the mapping of DNase protection fragment ends and measurement of STEM edge positions are alternative methods for observing the same binding events.

DISCUSSION

Significance of Bound Protein Structures Observed by STEM. The close correspondence between binding positions observed by STEM and by DNase protection indicates that

the STEM structures preexisted in solution. Our accompanying mass measurements show then that monomers, dimers, trimers, and tetramers occur in solution bound to the DNA so as to give protection against DNase for many minutes. Protein concentrations and molar ratios were chosen to show the full range of interactions between SV40 T antigen and the DNA origin of replication. Structures formed at low concentration may have relevance *in vivo*, in view of the increase from 0 of T-antigen concentration after infection.

At our highest T-antigen concentration and molar ratio, maximal binding structures in regions I and II occur. DNase protection experiments at this concentration and molar ratio develop the full range of protected fragments (Fig. 6), as observed in DNase protection experiments that systematically used a range of molar ratios extending to 120:1. If K_d in region I is 1 nM or less, as reported in the literature (15), our highest T-antigen concentration and molar ratio would insure saturation in region I. Further our observed binding frequencies (averaged over several concentrations) of 5, 9, and 10 for monomers, dimers, and trimers, respectively, imply approach to saturation. Therefore, if a fourth monomer site of comparable K_d existed in region I, occupation of the site would occur with appreciable frequency and tetramers would be observed. By similar argument, but at a somewhat lower confidence level statistically, a literature K_d for region II and our monomer-through-tetramer binding frequencies of 13, 11, 5, and 6 make a fifth comparable binding site in region II unlikely. The more surprising of the two results, namely trimer as maximal structure in region I, is strongly suggested by the data.

Significantly, the observed sharp cutoff in region I binding frequencies for mass greater than trimer is replaced by an equally sharp cutoff for mass greater than dimer when region I DNA is modified to reduce the number of proposed recognition sequences from 3 to 2 (unpublished data).

G-A-G-G-C as Recognition Sequence for the T-Antigen Monomer. It is clear from Figs. 3, 4, and 6 that the size of a T-antigen monomer is large compared to 5 bp. Therefore, the STEM data cannot by themselves establish G-A-G-G-C as a recognition sequence. However, it is interesting to examine the mass distributions of Figs. 4*D* and 5 (the same trimer/tetramer represented in two ways) and note that homologies exist between a dimer mass in region I and two dimer masses in region II; these have their parallel in pairs of G(T)-A-G-G-C sequences (Fig. 1). Further, the monomer appendage that creates the trimer in region I is on the same side of the dimer mass as the somewhat separated G-A-G-G-C sequence.

More generally, a variety of oligomeric states of T antigen bind stably to DNA origin sequences of SV40. It is most natural to suppose that they arise from binding of monomers to the same or similar recognition sequences. Seven closely similar pentanucleotides are found that could create the structures observed.

We thank D. Nathans and R. Dixon for cs1097 stock and K. Thompson of Brookhaven National Laboratory for the BMDP analysis. This work was funded by Grants CA-18808 and CA-28146 from the National Cancer Institute to P.T. Part of the work was supported also by National Institutes of Health Grant GM-30607 to P.V.C.H. and was performed under the auspices of the Department of Energy. The Brookhaven STEM is a National Institutes of Health Biotechnology Resource supported by Grant RR-00715 to J.W.

1. Tegtmeyer, P. (1975) *J. Virol.* **15,** 613–618.
2. Shortle, D. R., Margolskee, R. F. & Nathans, D. (1979) *Proc. Natl. Acad. Sci. USA* **76,** 6128–6131.
3. Tegtmeyer, P., Schwartz, M., Collins, J. K. & Rundell, K. (1975) *J. Virol.* **16,** 168–178.
4. Reed, S. I., Stark, G. R. & Alwine, J. C. (1976) *Proc. Natl. Acad. Sci. USA* **73,** 3083–3087.
5. Schaffhausen, B. (1982) *Crit. Rev. Biochem.* **13,** 215–286.
6. DePamphilis, M. L. & Wassarman, P. L. (1982) in *Organization and Replication of Viral DNA*, ed. Kaplan, A. S. (CRC Press, Cleveland, OH), pp. 37–114.
7. Tjian, R. (1981) *Curr. Top. Microbiol. Immunol.* **93,** 5–24.
8. Tjian, R. (1978) *Cold Spring Harbor Symp. Quant. Biol.* **43,** 655–662.
9. Shalloway, D., Kleinberger, T. & Livingston, D. M. (1980) *Cell* **20,** 411–422.
10. Tegtmeyer, P., Anderson, B., Shaw, S. B. & Wilson, V. W. (1981) *Virology* **115,** 75–87.
11. Meyers, R. M., Rio, D. C., Robbins, A. K. & Tjian, R. (1981) *Cell* **25,** 373–384.
12. Tegtmeyer, P., Lewton, B. A., DeLucia, A. L., Wilson, V. G. & Ryder, K. (1983) *J. Virol.* **46,** 151–161.
13. DeLucia, A. L., Lewton, B. A., Tjian, R. & Tegtmeyer, P. (1983) *J. Virol.* **46,** 143–150.
14. Tenen, D. G., Haines, L. & Livingston, D. M. (1982) *J. Mol. Biol.* **157,** 473–492.
15. Jones, K. A. & Tjian, R. (1984) *Cell* **36,** 155–162.
16. Myers, R. M., Williams, R. C. & Tjian, R. (1981) *J. Mol. Biol.* **148,** 347–353.
17. Bradley, M. K., Griffin, J. D. & Livingston, D. M. (1982) *Cell* **28,** 125–134.
18. Gidoni, D., Scheller, B. B., Hantzopoulos, P., Oren, M. & Prives, C. (1982) *J. Virol.* **42,** 456–466.
19. Fanning, E., Westphal, D.-H., Brauer, D. & Corlin, D. (1982) *EMBO J.* **1,** 1023–1028.
20. Hough, P. V. C., Mastrangelo, I. A., Wall, J. S., Hainfeld, J. F., Simon, M. N. & Manley, J. L. (1982) *J. Mol. Biol.* **160,** 375–386.
21. Wall, J. S. (1979) *Chem. Scripta* **14,** 271–278.
22. Wall, J. S. (1979) in *Introduction to Analytical Electron Microscopy*, eds. Hren, J. J., Goldstein, J. I. & Joy, D. C. (Plenum, New York), pp. 333–342.
23. Engel, A., Baumeister, W. & Saxton, W. O. (1982) *Proc. Natl. Acad. Sci. USA* **79,** 4050–4054.
24. Buchman, A. R., Burnett, L. & Berg, P. (1980) in *DNA Tumor Viruses*, ed. Tooze, J. (Cold Spring Harbor Laboratory, Cold Spring Harbor, NY), pp. 799–818.
25. DiMaio, D. & Nathans, D. (1982) *J. Mol. Biol.* **156,** 531–548.
26. Myers, R. M. & Tjian, R. (1980) *Proc. Natl. Acad. Sci. USA* **77,** 6491–6495.
27. Wilson, V. G., Tevethia, M. J., Lewton, B. A. & Tegtmeyer, P. (1982) *J. Virol.* **44,** 458–468.
28. Hansen, U., Tenen, D. G., Livingston, D. M. & Sharp, P. (1981) *Cell* **27,** 603–612.
29. Rio, D. C. & Tjian, R. (1983) *Cell* **32,** 1227–1240.
30. Benoist, C. & Chambon, P. (1981) *Nature (London)* **290,** 304–310.
31. Fromm, M. & Berg, P. (1982) *J. Mol. Appl. Genet.* **1,** 457–481.
32. Dynan, W. S. & Tjian, R. (1983) *Cell* **35,** 79–87.
33. Carroll, R. B., Hager, L. & Dulbecco, R. (1974) *Cold Spring Harbor Symp. Quant. Biol.* **34,** 291–293.
34. Tegtmeyer, P. & Andersen, B. (1981) *Virology* **115,** 67–74.
35. Mosesson, M. W., Hainfeld, J., Wall, J. & Haschemeyer, R. H. (1981) *J. Mol. Biol.* **153,** 695–718.
36. Wall, J. S., Hainfeld, J. F., Bartlet, P. A. & Singer, S. J. (1982) *Ultramicroscopy* **8,** 397–402.
37. Langmore, J. P., Wall, J. & Isaacson, M. S. (1973) *Optik* **38,** 335–350.
38. Frank, J. (1973) in *Advanced Techniques in Biological Electron Microscopy*, ed. Koehler, J. K. (Springer, Berlin), pp. 215–274.
39. Saxton, W. O. (1978) *Computer Techniques in Image Processing in Electron Microscopy* (Academic, New York), pp. 189–191.
40. Tenen, D. G., Taylor, T. S., Haines, L. L., Bradley, M. K., Martin, R. G. & Livingston, D. M. (1983) *J. Mol. Biol.* **168,** 791–808.